Polarimetric Imaging and Computational Techniques for Identification of Malignant Lesions

Mohammed Hachem MEZOUAR[1], Abdessamad ACHNAOUI[2], Mohammed TBOUDA[3], Said CHOUHAM[4], Said BELKACIM[5], Mohamed NEJMEDDINE[6], Driss MGHARAZ[7]
Laboratory of Cell Biology and Molecular Genetics, Ibnou Zohr University, Agadir, Morocco[1, 4, 6]
Materials, Signals, Systems and Physical Modeling Laboratory, Ibnou Zohr University, Agadir, Morocco[2, 7]
Faculty of Medicine and Pharmacy-Department of Anatomical Pathology, Oued Eddahab Military Hospital, Agadir, Morocco[3]
Laboratory of Applied Geology and Geo-Environment (LAGAGE), Ibnou Zohr University, Agadir, Morocco[5]

***Abstract*—According to the International Agency for Research on Cancer, cervical cancer is a major cause of death among Moroccan women, with high incidence and mortality rates. Early detection remains essential to increasing patients' chances of recovery. Our study combines polarized light imaging, digital image correlation (DIC), Gray-Level Co-occurrence Matrix (GLCM) texture analysis, and fractal-based local standard deviation mapping to identify microstructural alterations in cervical tissue. Smear and biopsy samples were collected and anonymized in hospitals in Agadir, Morocco. Our goal is to develop an optical system based on the interaction between polarized light and tissue, as well as a complementary computational framework to distinguish between different types of healthy, precancerous, and cancerous tissue. DIC revealed heterogeneous deformation patterns in cancerous regions, fractal analysis highlighted increased structural complexity, and GLCM features showed higher contrast and entropy in malignant samples. This pilot study introduces a novel approach combining polarimetric imaging and computational analysis, applied to cervical tissue samples from Moroccan women in Africa. Despite the small size of the ex vivo dataset, the results obtained encourage the conduct of larger-scale prospective and in vivo studies.**

***Keywords*—Polarized light; digital image correlation; Gray-Level Co-occurrence Matrix; fractal; cervix; cancer**

I. Introduction

Cervical cancer remains a major global public health concern, particularly in low- and middle-income countries (LMICs), where it represents one of the leading causes of cancer-related mortality among women. According to recent estimates from the World Health Organization and GLOBOCAN, more than 85% of cervical cancer deaths occur in these regions, largely due to late diagnosis and limited access to effective screening and early detection programs [1]. In North Africa, and specifically in Morocco, cervical cancer is among the most common gynecological malignancies, with incidence and mortality rates remaining high despite ongoing prevention efforts [2]. The cervical samples analyzed in the present study were obtained exclusively from Moroccan women, providing direct clinical relevance to this regional context.

In this context, one of the major challenges is the lack of screening tools that are simultaneously reliable, objective, cost-effective, and adaptable to constrained healthcare infrastructures. Conventional diagnostic approaches often rely on subjective visual assessment, requiring specialized expertise and equipment. This limits their scalability in environments with limited resources. In this regard, optical imaging techniques based on light polarization analysis offer a promising and innovative alternative. Polarimetric imaging is intrinsically sensitive to microstructural and organizational changes in biological tissues associated with early stages of carcinogenesis. Polarization-based methods can reveal subtle pathological alterations that are undetectable using conventional imaging techniques. This is achieved by examining the properties of anisotropy, scattering and structural organization.

In this work, we propose a computational framework based on polarimetric imaging for the analysis of cervical tissue samples, aiming to address current limitations to cervix screening. The proposed framework is well-suited for low-resource settings by combining availability, affordability and sensitivity to early microstructural alterations. The methodology integrates polarization analysis with advanced image processing and quantitative analysis methods, including digital image correlation (DIC), Gray-Level Co-occurrence Matrix (GLCM) analysis, and fractal analysis. The investigation of tissue architecture and organization enables discrimination between malignant and healthy regions, while texture analysis and structural complexity metrics provide quantitative biomarkers of early pathological alterations.

The main potential contributions of this study are threefold. First, the development of a polarimetric imaging framework specifically tailored for the characterization of cervical tissue in resource-limited settings. Second, the integration of polarization-derived parameters with multi-scale computational descriptors (DIC, GLCM, and fractal features) in order to achieve objective and quantitative tissue discrimination. Third, the experimental validation of the proposed approach using real ex vivo cervical tissue samples from anonymized Moroccan patients demonstrates its ability to reliably distinguish healthy tissue from malignant regions.

Building upon this framework, the present study first reviews related work on optical and polarization-based imaging techniques applied to cervical cancer detection. It then describes the experimental setup and materials, emphasizing a non-invasive, low-cost, and non-harmful imaging modality that

operates within the visible light spectrum and requires no contrast agents, in contrast to many conventional imaging techniques. The use of ex vivo cervical tissue samples is subsequently detailed, followed by a comprehensive presentation of the proposed computational methodology. The results are presented and discussed to demonstrate the robustness and effectiveness of the proposed framework to reliably distinguish healthy cervical tissue from malignant regions, highlighting its potential clinical relevance for early cancer detection and its contribution to reducing disparities in LMICs. Finally, the study ends with a conclusion.

II. Related Work

Polarization is a fundamental property of light and a powerful detection tool applied in many fields, including biomedical diagnosis. According to the literature, several works have been realized on the interaction between polarized light and tissue [3], [4], [5], [6]. In biomedical imaging, unlike non-polarized light, linear polarization is particularly useful for detecting early pathological changes due to the defined orientation of the electric field, which enhances sensitivity to tissue alteration and microstructural organization [7]. Different polarization measurement types have been used for cancer detection. For instance, in 2021, researchers at Tokyo Institute of Technology experimentally demonstrated a novel cancer diagnosis technique based on the scattering of circularly polarized light, which computational studies revealed can detect the progression of precancerous lesions and early cancer [8], [9].

In diagnostic applications, the interaction of polarized light with biological tissues provides valuable structural information, enhancing contrast, characterizing tissue, reducing surface reflections, and revealing subtle alterations for earlier and more accurate detection. Elliptically polarized light has demonstrated significant potential, offering complementary structural and compositional insights, while linearly polarized light [10] remains essential for reliable contrast enhancement and detailed assessment of tissue organization, and should not be overlooked.

Building on the ability of linearly polarized light to enhance contrast and reveal structural features, Orthogonal State Contrast (OSC) has emerged as a promising technique in biological imaging, and more broadly as a robust metric in laser-illuminated active polarimetric systems. Used as a practical surrogate for the degree of polarization, OSC enables efficient discrimination of targets with distinct polarimetric signatures, notably in remote sensing applications [11], [12].

Recent research has focused on refining Orthogonal State Contrast techniques to achieve higher precision in biological tissue analysis. For example, Pierangelo et al. analyzed cancerous and healthy human colon samples ex vivo using a multispectral Mueller polarimeter in the visible range (500–700 nm). Their study demonstrated that depolarization measurements under linearly polarized light depend on tumor presence, type, thickness, and tissue composition, allowing clear differentiation between healthy tissue, various tumor subtypes, and post-radiochemotherapy tissue. These results highlight the potential of polarization-based imaging for precise tissue characterization and rapid cancer staging [13].

Beyond colon studies, several investigations have applied Orthogonal State Contrast (OSC) and Mueller Matrix (MM) polarimetry to cervical tissue analysis. The cervix consists of squamous epithelium and connective tissue, with collagen fibers providing structural strength. Pathologies such as cervical intraepithelial neoplasia (CIN), cancer, pregnancy, and spontaneous preterm birth remodel both epithelial and connective layers. OSC and MM polarimetry, using polarized light, enable quantification of these changes, with parameters like depolarization and birefringence providing contrast linked to tissue organization and pathology. Advances in OSC-based imaging, including specialized colposcopes, support detailed, non-invasive assessment of cervical alterations, highlighting the potential of polarization techniques for early detection and clinical diagnostics [14].

Leveraging the benefits of polarized light for enhancing tissue contrast and revealing structural features, fractal analysis has emerged as a powerful tool for cancer detection. By quantifying the complexity of tissue architecture, fractal dimension measures can distinguish malignant regions from healthy tissues, capturing subtle morphological alterations that are often invisible to conventional imaging [15]. Complementing this, Gray-Level Co-occurrence Matrix (GLCM) analysis provides quantitative information about tissue texture, such as contrast, correlation, and homogeneity, which has been successfully applied to differentiate cancerous from normal cells in various tissue types [16], [17]. The combination of polarized light imaging and computational analysis offers a reliable and objective approach for early malignancy detection, highlighting its promise in non-invasive cancer diagnostics.

Motivated by previous research, this work employs polarized light imaging combined with computational techniques to analyze cervical tissue samples. The next section details the experimental approach, covering sample handling, imaging procedures, and computational analysis for tissue classification.

III. Materials and Methods

A. Instruments and Measurement Protocol

We studied the interaction of histological slides of the cervix with polarized light on a microscopic level. This approach, known as polarization microscopy, can reveal detailed structural information about tissue. The optical setup employs a commercially available polarized light microscope (OPTIKA, Italy) to enable detailed observation and analysis of microscopic structures, revealing intricate details and providing insights across various scientific disciplines. For polarized light observations, a polarizer and an analyzer were used, and for image acquisition, a charge-coupled device (CCD) camera (OPTIKA C-B18+, SN 621237) was employed.

1) Equipment and imaging setup: The biological samples must be prepared in a specific manner to minimize diffusion and irrelevant absorption, and to avoid any optical aberrations that could introduce intensity variations or polarization-related artifacts. The microscope is directly connected to a dedicated computer for real-time image acquisition and data analysis.

The CCD camera is mounted via a C-mount adapter on the trinocular port; it captures images and transmits them to the computer for processing in MATLAB.

2) Camera specifications: The imaging system was equipped with a high-resolution OPTIKA CCD camera (SN 621237) to capture detailed microstructural features. The camera sensor provides a resolution of 4912 × 3684 pixels (18 MP) with an Aptina color CMOS sensor of 1/2.3″ and a pixel size of 1.25 µm, allowing for high-detail imaging. The frame rate reaches up to 5.6 fps at full resolution and up to 32.2 fps at 1228 × 922 resolution, facilitating rapid positioning of samples. The bit depth is configurable from 1 to 24 bits, with 8–12-bit A/D conversion ensuring accurate color fidelity. An integrated IR-CUT filter (380–650 nm) minimizes infrared interference, and the camera is compatible with Windows, macOS, and Linux via ProView and Liteview software.

3) Image acquisition under parallel polarized light: The experimental procedure began with sample preparation and ROI selection, where thin sections were carefully placed on the mechanical stage, and regions of interest (ROIs) were visually identified through the eyepiece. For polarization measurements, incident light passed sequentially through a linear polarizer, the sample, and a linear analyzer aligned parallel to the polarizer, allowing the acquisition of intensity images under parallel-polarized conditions. Image capture was performed using an OPTIKA camera controlled via ProView, with exposure and gain adjusted to prevent saturation. Finally, the acquired images were processed in MATLAB to extract quantitative information about local structural variations. Maps of intensity changes were generated, highlighting subtle alterations in tissue organization and optical properties, thereby enabling a detailed assessment of microstructural features and their spatial distribution.

4) Methodological overview: The optical behavior of a sample under complete polarization can be described by a 4×4 Mueller matrix, requiring 16 independent intensity measurements for fully characterizing diattenuation, retardance, and depolarization [18]. In this study, the measurements are limited to a linear polarization (parallel polarizer/analyzer). To simplify the analysis, we exclude from consideration circular or depolarizing effects to reduce acquisition time and computational complexity. Such an approach has been proven in prior studies using reduced 3×3 Mueller-matrix decomposition for quantitative tissue polarimetry [19], [20].

B. Sample Preparation

Histological samples are prepared through standardized and sequential procedures to preserve tissue architecture and enable microscopic examination. The typical steps include tissue collection, fixation, dehydration, clearing, embedding, sectioning, mounting, staining, cover slipping and final microscopic evaluation. These histological procedures ensure good-quality sections suitable for reliable optical analysis [21].

The actual specimens used in this study were obtained from the Pathological Anatomy Laboratory of the Faculty of Medicine and Pharmacy of Agadir. Fig. 1 presents representative cervical tissue sections: infiltrating tumor (left, number 559) and healthy tissue (right, number 332). The black rectangles indicate the regions of interest (ROIs) selected for quantitative analysis under polarized light.

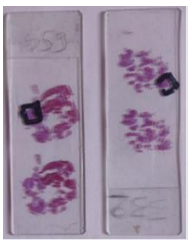

Fig. 1. Cervical tissue samples: cancerous specimen (left) and healthy specimen (right). Black boxes indicate the ROIs selected for analysis.

Fig. 2 establishes the link between the preparation process and the anonymized samples used in our study, highlighting the importance of adequate tissue preparation for polarimetric imaging analysis.

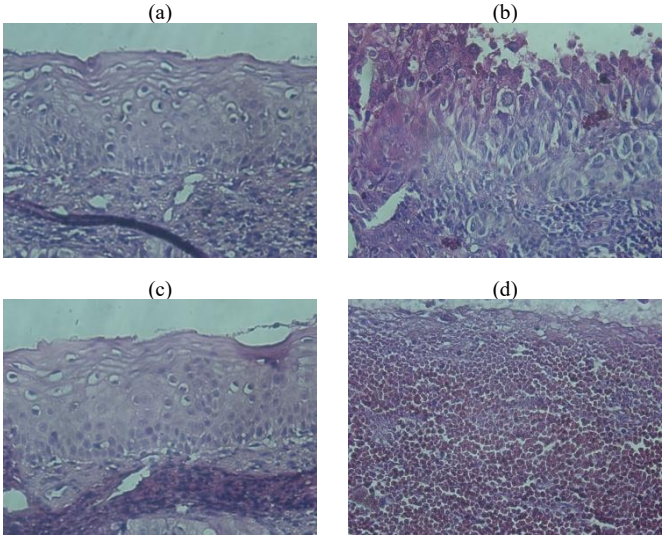

Fig. 2. Epithelial region of cervical tissue under 400× magnification with parallel polarized light. (a, c) healthy tissue and (b, d) invasive cancer.

C. Orthogonal State Contrast and Stokes-Mueller Formalism

Since the early 1990s, the polarimetry technique has been applied to study biological tissues, initially in dermatology. In 1991, R. Anderson introduced a pioneering approach using polarizers and filters to eliminate surface specular reflections during the imaging of human skin, thereby improving lesion visibility [22]. Further developments polished this strategy by using linearly polarized light to illuminate damaged tissue, and analyzing the returned light in the orthogonal polarization state [23].

In 2002, the configuration proposed by S. L. Jacques et al. improved the imaging of pathological skin regions. Their system included a two-state analyzer alternately aligned parallel or perpendicular to the incident polarization. This property made it possible to extract pixel-by-pixel orientation-dependent intensity maps [24]. Similar approaches based on two orthogonal linear polarization states produced images

comparable to linear polarization degree maps, enabling rapid contrast enhancement in low-scattering tissues [25].

In this work, the adoption of polarimetric imaging was motivated by the robustness of the Stokes-Mueller formalism [26], [27], [28] for two main reasons:

- It relies entirely on optical intensities, as these can be measured directly in experiments.
- It has a natural aptitude for partially polarized light, a situation that occurs frequently due to multiple scattering and structural heterogeneities in biological tissues.

The polarization state of light is represented by a Stokes vector:

$$S= [S_0, S_1, S_2, S_3]^T$$

where, S_0 represents the total intensity, S_1 and S_2 describe the linear polarization components, and S_3 corresponds to the circular polarization component. For analysis purposes, the Stokes vector is often normalized by its total intensity:

$$\left[\frac{S_0}{S_0}, \frac{S_1}{S_0}, \frac{S_2}{S_0}, \frac{S_3}{S_0}\right]^T = [1, S_1, S_2, S_3]^T \quad (1)$$

The Mueller matrix, M, characterizes the complete polarimetric response of a sample by mapping the input Stokes vector to the output vector. In normalized form, its elements are expressed as:

$$M = \begin{bmatrix} 1 & m12 & m13 & m14 \\ m21 & m22 & m23 & m24 \\ m31 & m32 & m33 & m34 \\ m41 & m42 & m43 & m44 \end{bmatrix} \quad (2)$$

where, mij = Mij / M11.

The element M_{11} quantifies attenuation for an unpolarized incident beam. For completely unpolarized illumination ($S_1 = S_2 = S_3 = 0$), the outgoing intensity reduces to:

$$S'_0 = M11\ S_0$$

This formalism provides a comprehensive description of the interaction between light and biological tissues, which are heterogeneous and highly scattering media. This is allowing each matrix element to be interpreted in terms of diattenuation, retardance, depolarization and structural anisotropy.

Based on this approach, polarimetric imaging has become a highly effective research tool for analyzing the microstructural properties of tissues. The combination of its major advantages makes it particularly relevant, such as improved contrast, high sensitivity to anisotropies, and its non-invasive nature, which are essential qualities for the early detection of tissue abnormalities. Moreover, recent studies have confirmed the utility of Mueller polarimetry in the detection of cancer in cervical tissue specimens, whether in the laboratory (ex vivo) or directly on the patient (in vivo) [29], [30], [31], [32].

In this study, the configuration chosen is simple and accessible, with linear polarimetry using a simple parallel[1] polarizer-analyzer setup. Without the need for more complex circular and elliptical analysis, this approach is more than sufficient for us to observe the essential effects related to polarization. Our method is based on combining the simplified optical system with state-of-the-art computer image processing. This allows us to extract markers that provide information on the architecture, texture, and complexity of the structure. These multimodal optical and image descriptors significantly improve the sensitivity and objectivity of our diagnosis, as they are closely linked to the microscopic remodeling typical of cancer development.

IV. Results

A. Digital Image Correlation

Digital Image Correlation (DIC) is an optical technique used to measure the full-field deformation, and is used in several applications (biological tissues, metals…). It is a powerful method because it can detect the most subtle structural changes and deformation patterns within images. Unlike traditional pixel-based comparisons, digital image correlation tracks local texture variations to measure displacement with high spatial accuracy, even at the microscopic scale. This is particularly useful in biomedical imaging, where subtle mechanical differences between healthy and abnormal tissues can be identified at an early stage by analyzing their deformation [33], [34], [35].

Concerning DIC analysis, two strictly identical regions of interest (ROIs), one healthy and one cancerous, were selected. Fig. 3 shows the statistical distribution of strain magnitudes, established by taking the reference ROI as the healthy sample, while the cancerous sample was analyzed using the same ROI dimensions. The histogram is clearly skewed to the left. Most of the points are concentrated around high deformation values (around 8–9 on the x-axis). In addition, the histogram exhibits a very sharp peak with a frequency close to 3.5×10^4 for a deformation magnitude of 8.5 to 9. This peak highlights a dominant deformability in the analyzed region, revealing mechanically weakened and highly altered tissue, indicating the presence of anomalous areas. Further insight is provided by Fig. 4, which illustrates the microscopic displacement vectors, revealing spatial variations in tissue deformation and highlighting underlying tissue heterogeneity.

Our future work will focus on analyzing tissue samples from the same patient over an extended period of time, maintaining a consistent ROI in order to track the chronological evolution of local deformations. Although this approach is technically demanding, establishing collaborations with hospitals and obtaining patient consent would enable longitudinal studies to be conducted, particularly in the context of cervical cancer. Such datasets would facilitate a more accurate characterization of the mechanical changes that occur during the progression of the disease.

[1] For a first-stage study of cervical cancer, the parallel-polarizer configuration is sufficient because it captures co-polarized light that highlights differences in tissue scattering and structure between normal and malignant regions, providing clear contrast with simple and rapid acquisition.

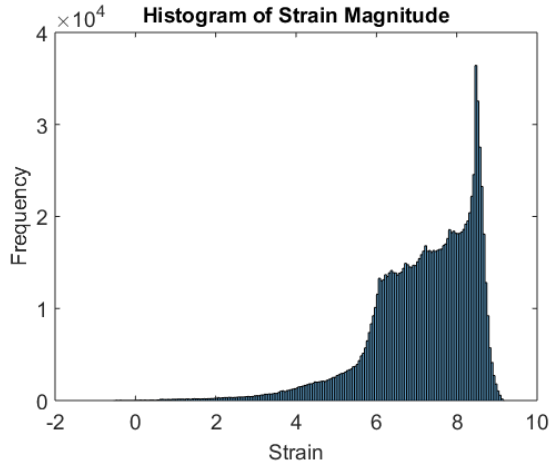

Fig. 3. Histogram of local strain magnitude in cervical epithelium via DIC.

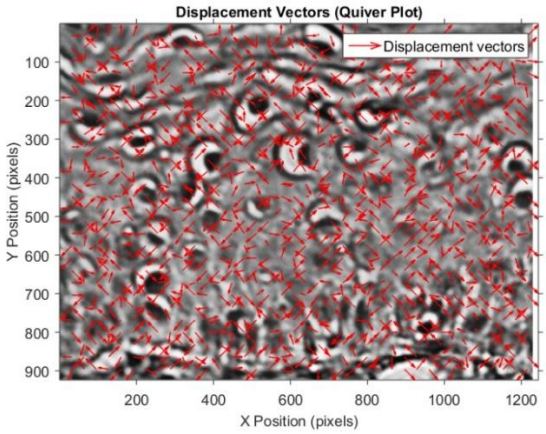

Fig. 4. Microscopic displacement vectors highlighting tissue heterogeneity.

The interpretation of these findings will be presented in the next section. Following the biomechanical insights from DIC, fractal analysis was applied to capture variations in tissue architectural complexity, providing complementary information on microstructural heterogeneity.

B. Fractal Dimension Measurement

Fractal analysis quantifies the degree of complexity and self-similarity of biological tissues, thus capturing tissue heterogeneity at different scales. In biomedical research, this technique is used to evaluate tumor morphology, epithelial organization and microvascular networks, providing information about pathological alterations that are difficult to detect using standard imaging techniques [36], [37], [38], [39], [40].

For this analysis, we applied the Fractal Map Analysis (FMA) approach on microscopic images. To achieve this, we used the local standard deviation (StdDev) to evaluate the structural complexity, because it is highly sensitive to spatial variations and irregularities. The images were first pre-processed (median filtering, contrast enhancement, and slight Gaussian smoothing). We then computed a high-resolution local standard deviation map to quantify spatial heterogeneity. The distribution was analyzed using histograms and statistical markers (mean, median, maximum, 90th percentile) to characterize tissue complexity, differentiating healthy from cancerous regions.

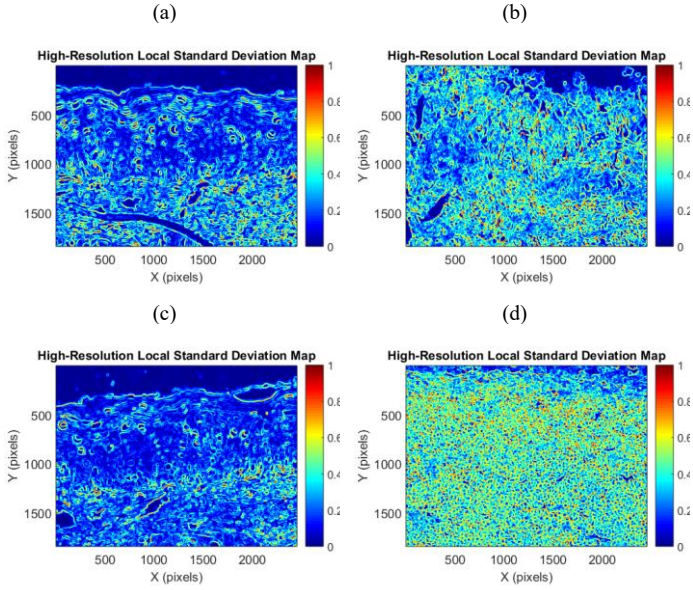

Fig. 5. Quantitative standard deviation maps of epithelial tissue: (a, c) healthy regions and (b, d) cancerous regions.

Fig. 5 illustrates the results of applying the fractal complexity map to the samples under parallel-polarized light, while Fig. 6 shows the corresponding histograms for each sample. In this study, fractal analysis was performed using the standard deviation of the complexity map to quantify tissue heterogeneity. While this approach effectively highlights differences between healthy and cancerous tissues, other fractal analysis methods, such as the box-counting method, could be explored in future work to provide complementary insights and potentially enhance diagnostic accuracy.

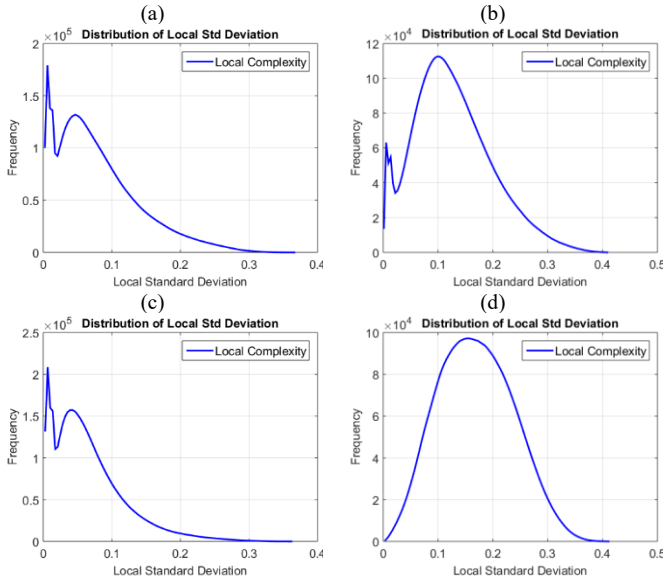

Fig. 6. Distribution of tissue complexity via fractal-based standard deviation. (a, c) healthy tissue and (b, d) invasive cancer.

Fractal analysis revealed marked differences in structural complexity between healthy and cancerous tissues. To further characterize local variations, GLCM analysis was applied, capturing variations in texture such as contrast, correlation, energy, and entropy, which provide additional quantitative indicators to distinguish healthy from malignant regions.

C. Gray-Level Co-occurrence Matrix Texture Features

Texture analysis is essential for characterizing tissue microstructure. The GLCM quantifies spatial relationships between pixel intensities, providing quantitative markers to distinguish healthy from pathological regions.

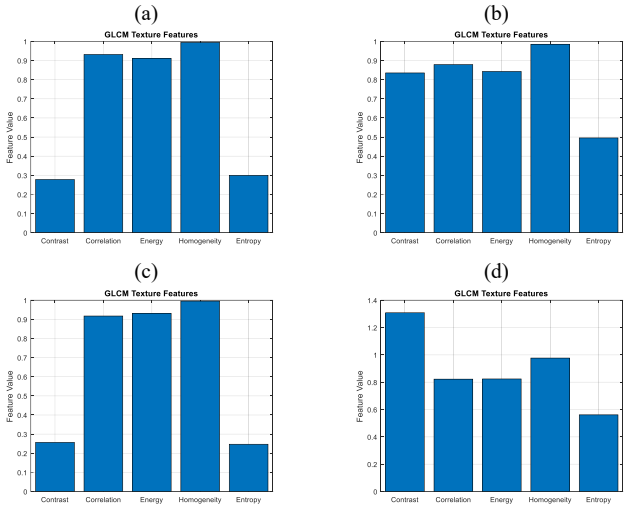

Fig. 7. GLCM-derived correlation, energy, homogeneity, entropy, and contrast maps: (a, c) healthy samples and (b, d) malignant samples.

In biomedical imaging, GLCM is widely used to characterize the microstructure of biological tissues (such as the cervix), since subtle differences in cell arrangement, nuclear chromatin, or extracellular matrix produce measurable variations in texture [41], [42], [43], [44]. In Fig. 7, the metrics are displayed in the following order: contrast, correlation, energy, homogeneity, and entropy, with each represented by a separate bar corresponding to this sequence, providing a clear and quantitative comparison of tissue texture.

The GLCM analysis presented in Fig. 7 highlights clear differences in texture between healthy and cancerous tissue samples. For the two healthy samples, correlation, homogeneity, and energy are all very high (≈0.92–0.99), while contrast and entropy are low (≈0.25–0.30), indicating a highly uniform and regular microstructure with minimal local intensity variation, typical of normal epithelial tissue.

In contrast, the cancerous samples exhibit markedly increased contrast (0.83–1.31) and entropy (0.50–0.56), reflecting greater heterogeneity and structural disorder in the tissue. Correlation, energy, and homogeneity are reduced compared to healthy tissue, indicating that pixel intensities are less spatially coherent and more irregular, potentially consistent with the disrupted cellular architecture found in malignant epithelium. Notably, sample “d” shows the highest contrast and entropy, suggesting the most pronounced microstructural heterogeneity among the cancerous tissues analyzed.

TABLE I. GLCM TEXTURE: HEALTHY VS. CANCEROUS.

GLCM texture features	Healthy sample "a"	Healthy sample "c"	Cancerous sample "b"	Cancerous sample "d"
Contrast	0.2780	0.2568	0.8351	1.3082
Correlation	0.9316	0.9173	0.8785	0.8223
Energy	0.9115	0.9314	0.8429	0.8238
Entropy	0.3002	0.2471	0.4955	0.5610
Homogeneity	0.9950	0.9954	0.9851	0.9766

Overall, these results, as shown in Table I, confirm that GLCM-derived texture features effectively capture the increased randomness and decreased uniformity associated with pathological epithelial tissue, making them valuable markers for distinguishing healthy from cancerous regions.

V. DISCUSSION

A. Digital Image Correlation

As shown in Fig. 3, the strain-magnitude histogram provides a statistical view of local deformation distribution within the ROI. Each DIC block contributes a displacement magnitude $\left(U_x^2 + U_y^2\right)^{0.5}$, and these values are grouped into bins to represent their frequency. The presence of higher frequencies at large strain values indicates that a significant portion of the ROI is undergoing solid local deformation. As the results show, this distribution exhibits accentuated heterogeneity, indicating irregularity and weakening of the tissue structure, which may reveal abnormal behavior. In biomedical imaging, such a distribution is generally associated with pathological regions where altered microarchitecture causes increased and widespread deformation.

Fig. 4 displays the filtered reference ROI (healthy region) overlaid with red displacement vectors computed by DIC. Each arrow characterizes the local motion of a small image block: its direction indicates how the tissue moved between the reference (healthy tissue) and deformed states (invasive tumor), and its length reflects the displacement magnitude. Variations in arrow orientation and magnitude provide a spatial visualization of how different regions within the tissue deform.

The heterogeneous orientations and amplitudes of the vectors reveal non-uniform deformation across the ROI. Regions with long arrows correspond to strong local displacement, while short arrows indicate nearly static areas. In our case, the displacement field shows pronounced and irregular motion, consistent with mechanically abnormal tissue. The strain indicators (mean ≈ 7.2 px, median ≈ 7.8 px, 90th percentile ≈ 8.5 px) confirm the presence of high-magnitude deformation, supporting the interpretation of increased structural heterogeneity typically associated with malignant regions.

In summary, DIC provides a rapid, non-invasive, and highly precise method for capturing local tissue deformation, generating detailed displacement and stress maps that reveal

mechanical heterogeneity. Its primary diagnostic value lies in detecting subtle biomechanical abnormalities, making it a powerful tool for distinguishing between healthy and cancerous tissue. Complementing this, fractal analysis characterizes the architectural complexity and heterogeneity of tissue structures, offering unique insights into morphological irregularities. Together, these modalities provide distinct and complementary diagnostic information, each contributing a unique perspective to tissue characterization.

B. Fractal Dimension Measurement

Fig. 5 presents the spatial standard deviation maps, which reveal clear differences in tissue heterogeneity between healthy and cancerous samples, particularly within the epithelial region. Healthy tissues show high uniformity, with most values clustered around low standard deviations (mean ≈ 0.07–0.08, 90th percentile ≈ 0.14–0.17), corresponding to the predominantly blue areas on the color map, indicating homogeneous microstructure. In contrast, cancerous tissues exhibit markedly higher and more variable local standard deviations (mean ≈ 0.13–0.17, 90th percentile ≈ 0.23–0.26), with color maps showing scattered regions of blue, green, yellow, and orange. This reflects increased structural heterogeneity and irregularity in the epithelium, consistent with disrupted cellular architecture. The cancerous sample “d” illustrates the most pronounced variability and the highest local complexity.

Fig. 6 presents the distribution of local Std Dev for 4 specimens of cervical epithelium (two healthy, and two cancerous). This measure is used to quantify the structural complexity of tissue using FMA. As illustrated in Fig. 6, the histograms of the local standard deviation quantitatively confirm the observations made on the complexity maps. The healthy samples ("a" and "c") show narrow distributions, strongly skewed toward low values (≈0.07–0.08 mean), reflecting a uniform and consistent tissue structure. The cancer samples ("b" and "d"), on the other hand, show wider distributions with higher median and 90th percentile values (≈0.13–0.17 mean, 0.23–0.26 90th percentile), indicating greater local variability and increased structural complexity. These histogram profiles support the idea that malignant epithelial regions are significantly more heterogeneous and disorganized than healthy tissue.

In conclusion, local standard deviation analysis is an effective method for quantifying tissue heterogeneity. Healthy epithelium exhibits low variability and a uniform structure, while cancerous regions display higher and more dispersed local standard deviations, reflecting increased structural complexity. This method therefore provides a quantitative and sensitive measure for distinguishing healthy tissue from malignant tissue.

While fractal analysis highlights the architectural complexity of tissues, GLCM-based texture analysis quantitatively captures microstructural variations in pixel intensity. Combined with polarized light, these methods provide complementary diagnostic information: fractal analysis reveals structural heterogeneity, whereas GLCM metrics, including contrast, entropy, correlation, energy and homogeneity, objectively characterize microstructural patterns, each offering distinct insights into tissue characterization.

C. Gray-Level Co-occurrence Matrix Texture Features

Fig. 7 and Table I show that GLCM metrics effectively distinguish non-neoplastic from neoplastic tissue. Healthy samples display high correlation, homogeneity, and energy with low contrast and entropy, indicating a uniform microstructure. Conversely, cancerous tissues exhibit elevated contrast and entropy with reduced correlation and energy, reflecting structural heterogeneity and disorganization. These quantitative differences provide clear markers for differentiating normal and malignant regions.

Fig. 8 shows the entropy distribution and confirms the heterogeneity of the tissues by introducing a measure of disorder and texture complexity. When the healthy samples are considered (red and blue curves), we observe narrower distributions concentrated around low modal values (between 0.35 and 0.45), indicating low dispersion of local pixel intensities and characteristic of an organized and homogeneous tissue structure. In contrast, tumoral samples (green and magenta curves) show wider distributions, with a mode significantly shifted toward higher entropy values (up to approximately 0.65 for sample “d”). This spread and alteration indicate an overall increased microstructural disorder and local complexity. This entropic marker thus reinforces the conclusions drawn from the fractal analysis, as entropy is strongly correlated with fractal dimension.

Entropy allows for highly sensitive quantitative measurement of pathological conditions. Despite a slight overlap between the distributions of samples a and b (healthy and cancerous, respectively), analysis of the statistical parameters of the distribution makes it possible to quantify the degree of tissue disorder and effectively use this metric as a multimodal descriptor for classification.

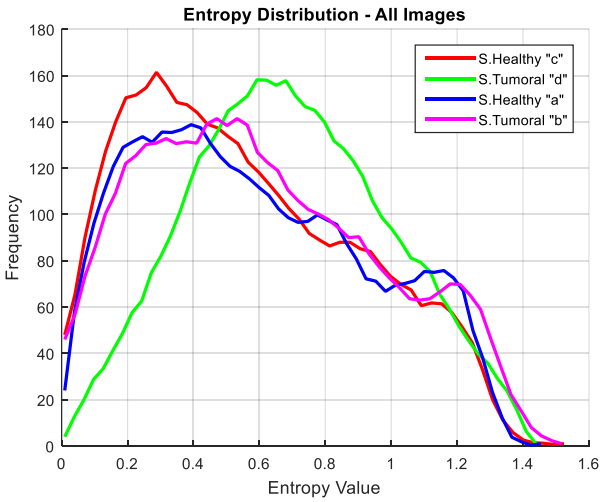

Fig. 8. Histogram of GLCM entropy in four cervical tissue samples.

Collectively, the GLCM analysis clearly differentiates healthy from tumorous epithelial tissue. Healthy samples exhibit high correlation, homogeneity, and energy with low contrast and entropy, indicating a uniform and regular

microstructure. Cancerous samples show markedly increased contrast and entropy alongside reduced correlation, energy, and homogeneity, reflecting greater structural heterogeneity and disorganization. The progressive increase in entropy from healthy to cancerous samples demonstrates the sensitivity of GLCM-derived features in detecting gradual changes in tissue architecture associated with malignancy.

Although the ex vivo dataset in the present study was limited in size, the results are highly promising and highlight the need for larger-scale prospective and in vivo investigations. Addressing the current limitations would allow for more robust validation of the findings, a comprehensive assessment of inter-patient variability, and a deeper understanding of the feasibility and translational potential of these imaging techniques in clinical practice. Future studies will focus on expanding the sample size, incorporating diverse patient populations, and optimizing the methodologies for in vivo application. Such efforts are critical to bridge the gap between experimental observations and practical diagnostic implementation, ultimately facilitating the translation of these techniques into routine clinical care.

To summarize, polarized light imaging was combined with computational techniques, including DIC, GLCM, and fractal analysis, to characterize cervical tissue microstructure. The key findings from these complementary approaches are outlined in Table II, providing an integrated overview of the most relevant imaging indicators for distinguishing healthy from malignant tissue.

TABLE II. SUMMARY OF KEY IMAGING INDICATORS

Indicators / Metrics	DIC (Displacement Magnitude)	Fractal (StdDev)	GLCM Metrics
Mean	7.2px →confirm the presence of high-magnitude deformation.	0.07–0.08 (Healthy). 0.13–0.17 (Cancerous).	-Contrast: 0.25–0.30 (Healthy), 0.83–1.31 (Cancerous). -Entropy: 0.25–0.30 (Healthy), 0.50–0.56 (Cancerous).
Median/90th Percentile	Median ≈ 7.8 px 90th ≈ 8.5 px	90th: 0.14-0.17 (Healthy). 90th: 0.23–0.26 (Cancerous).	Energy: 0.91–0.93 (Healthy). 0.82–0.87 (Cancerous).
Analysis	High strain → mechanically altered tissue	Low StdDev →uniform (healthy). High StdDev →Irregular (cancer).	Healthy tissue → uniform, low contrast / entropy. Cancerous tissue →disordered, high contrast / entropy.

VI. CONCLUSION

Cervical cancer remains a leading cause of cancer-related mortality among women worldwide, particularly in low Human Development Index countries. Despite advances in screening and treatment, early detection is critical to improving outcomes. Polarimetric imaging with digital analysis methods has emerged as a promising tool for enhancing diagnostic accuracy by characterizing structural properties of biological tissues. This study investigates early diagnosis of cervical cancer in Moroccan women, using computational polarimetric imaging to differentiate healthy from malignant tissue. Combined analyses with DIC, GLCM texture, and fractal-based local standard deviation consistently reveal clear distinctions; healthy tissue shows low texture entropy, high correlation and homogeneity, and minimal local variability, whereas cancerous tissue exhibits random, multidirectional deformation patterns, increased contrast and entropy, reduced correlation and homogeneity, and higher local variability. These quantitative imaging biomarkers provide a robust framework for detecting and characterizing malignant changes. Building on these findings, future work will focus on validating the diagnostic performance and clinical applicability of this approach using full Mueller Matrix measurements on intact cervical specimens from a diverse patient cohort. Key challenges for clinical translation, including in vivo acquisition where motion artifacts and tissue accessibility must be managed, patient variability in anatomy and tissue properties, and instrumentation costs related to complex polarimetric setups, will be addressed. In addition, machine learning classifiers, such as support vector machines and convolutional neural networks, will be explored for multimodal feature fusion to enhance diagnostic accuracy and enable robust, automated tissue classification.

ACKNOWLEDGMENT

The authors express their sincere gratitude to Prof. Aziz Zentar, Head Doctor of the Moulay Ismail Military Hospital in Meknes, and Prof. Ahmed Belmouden, Dean of the Faculty of Sciences, Ibnou Zohr University, Agadir, for their guidance and continuous support. Special appreciation is extended to Prof. Mohamed Benyahya for his constructive advice. The authors also thank Dr. Abdelali Benali, Specialist in Anatomic Pathology, Biomedical Engineer Youness El Ouahabi, and Mr. Rachid Razine for their valuable assistance throughout the study.

AI USE STATEMENT

Generative AI was used only for language editing. All ideas, analyses, and conclusions were produced and verified by the authors.

REFERENCES

[1] F. Bray et al., « Global cancer statistics 2022: GLOBOCAN estimates of incidence and mortality worldwide for 36 cancers in 185 countries », CA. Cancer J. Clin., vol. 74, no 3, p. 229-263, 2024, doi: 10.3322/caac.21834.

[2] M. Allali et al., « Cervical cancer in Morocco: a literature review on risk factors, prevalence, and healthcare challenges », Pan Afr. Med. J., vol. 50, p. 11, jan. 2025, doi: 10.11604/pamj.2025.50.11.43975.

[3] J. Kim, R. John, P. J. Wu, M. C. Martini, et J. T. Walsh, « In vivo characterization of human pigmented lesions by degree of linear polarization image maps using incident linearly polarized light », Lasers Surg. Med., vol. 42, no 1, p. 76-85, jan. 2010, doi: 10.1002/lsm.20866.

[4] W. Wang, L. G. Lim, S. Srivastava, J. S. B. Yan, A. Shabbir, et Q. Liu, « Roles of linear and circular polarization properties and effect of wavelength choice on differentiation between ex vivo normal and

cancerous gastric samples », J. Biomed. Opt., vol. 19, no 4, p. 046020, apr. 2014, doi: 10.1117/1.JBO.19.4.046020.

[5] S. N. Tukimin, S. B. Karman, M. Y. Ahmad, et W. S. Wan Kamarul Zaman, « Polarized Light-Based Cancer Cell Detection Techniques: A Review », IEEE Sens. J., vol. 19, no 20, p. 9010-9025, oct. 2019, doi: 10.1109/JSEN.2019.2924535.

[6] A. H. Hielscher, A. A. Eick, J. R. Mourant, J. P. Freyer, et I. J. Bigio, « Biomedical diagnostic with diffusely backscattered linearly and circularly polarized light », in Biomedical Sensing, Imaging, and Tracking Technologies II, SPIE, jun 1997, p. 298-305. doi: 10.1117/12.275538.

[7] W. Liu et al., « Effect of linearly polarized light irradiation near stellate ganglion on postoperative sleep disorders in patients undergoing modified radical mastectomy of breast cancer », Perioper. Med., vol. 14, no 1, p. 113, oct. 2025, doi: 10.1186/s13741-025-00601-0.

[8] V. Dremin et al., « Imaging of early stage breast cancer with circularly polarized light », présenté à Tissue Optics and Photonics, apr. 2020, p. 1136304. doi: 10.1117/12.2554166.

[9] N. Nishizawa, B. Al-Qadi, et T. Kuchimaru, « Angular optimization for cancer identification with circularly polarized light », J. Biophotonics, vol. 14, no 3, p. e202000380, 2021, doi: 10.1002/jbio.202000380.

[10] R. Ceolato, M. Golzio, C. Riou, X. Orlik, et N. Riviere, « Spectral degree of linear polarization of light from healthy skin and melanoma », Opt. Express, vol. 23, no 10, p. 13605-13612, may 2015, doi: 10.1364/OE.23.013605.

[11] J. Dupont, M. Boffety, et F. Goudail, « Precision of polarimetric orthogonal state contrast estimation in coherent images corrupted by speckle, Poisson, and additive noise », JOSA Vol 35 Issue 6 Pp 977-984, jun 2018, doi: 10.1364/JOSAA.35.000977.

[12] L. Rey-Barroso et al., « Polarized Multispectral Imaging for the Diagnosis of Skin Cancer », Color Imaging Conf., vol. 27, p. 381-385, oct. 2019, doi: 10.2352/issn.2169-2629.2019.27.68.

[13] A. Pierangelo et al., « Ex-vivo characterization of human colon cancer by Mueller polarimetric imaging », Opt. Express, vol. 19, no 2, p. 1582-1593, jan. 2011, doi: 10.1364/OE.19.001582.

[14] S. Khan, M. Qadir, A. Khalid, S. Ashraf, et I. Ahmad, « Characterization of cervical tissue using Mueller matrix polarimetry », Lasers Med. Sci., vol. 38, no 1, p. 46, jan. 2023, doi: 10.1007/s10103-023-03712-6.

[15] Y. Zhang, M. Chen, L. Man, G. Lin, et Y. Qian, « Study on Skin Cancer Classification Based on Image Fractal Dimension », in 2024 International Conference on Energy and Electrical Engineering (EEE), jul. 2024, p. 1-3. doi: 10.1109/EEE59956.2024.10709720.

[16] M. Mawarni, F. Utaminingrum, et W. F. Mahmudy, « The Effect of Feature Selection on Gray Level Co-Occurrence Matrix (GLCM) for the Four Breast Cancer Classifications », J. Biomim. Biomater. Biomed. Eng., vol. 55, p. 168-179, 2022, doi: 10.4028/p-09g3n8.

[17] H. H. Fauziah, D. R. Ningtias, B. Wahyudi, et J. N. Simanjuntak, « Identification of lung cancer using gray level co-occurrence matrix (GLCM) and artificial neural network with backpropagation algorithm », J. Soft Comput. Explor., vol. 6, no 1, p. 51-61, apr. 2025, doi: 10.52465/joscex.v6i1.543.

[18] E. Nabadda, M. del M. Sánchez-López, A. Vargas, A. Lizana, J. Campos, et I. Moreno, « Mueller matrix imaging polarimeter with polarization camera self-calibration applied to structured light components », J. Eur. Opt. Soc.-Rapid Publ., vol. 20, no 1, p. 5, 2024, doi: 10.1051/jeos/2024003.

[19] H. Wei, Y. Zhou, L. Ren, et F. Ma, « Optimal Orientation Angle Configuration of Polarizers Exists in a 3 × 3 Mueller Matrix Polarimeter », Photonics, vol. 10, no 10, p. 1087, oct. 2023, doi: 10.3390/photonics10101087.

[20] Z. Huang, Y. Fu, Z. Li, et J. Wu, « A Portable 3×3 Mueller Matrix Polarimeter Prototype for Cancer Detection Ex Vivo », in Proceedings of the 3rd International Conference on Biomedical Signal and Image Processing, in ICBIP '18. New York, NY, USA: Association for Computing Machinery, aug. 2018, p. 92-97. doi: 10.1145/3278229.3278244.

[21] S. M, B. Al, et F. L, « Tissue Sampling and Processing for Histopathology Evaluation. », Methods Mol. Biol. Clifton NJ, vol. 1641, p. 101-114, jan. 2017, doi: 10.1007/978-1-4939-7172-5_4.

[22] R. R. Anderson, « Polarized light examination and photography of the skin », Arch. Dermatol., vol. 127, no 7, p. 1000-1005, jul. 1991. doi:10.1001/archderm.1991.01680060074007.

[23] S. M. Milner, S. Bhat, S. Gulati, G. Gherardini, C. E. Smith, et R. J. Bick, « Observations on the microcirculation of the human burn wound using orthogonal polarization spectral imaging », Burns J. Int. Soc. Burn Inj., vol. 31, no 3, p. 316-319, may 2005, doi: 10.1016/j.burns.2004.10.014.

[24] S. L. Jacques, J. C. Ramella-Roman, et K. Lee, « Imaging skin pathology with polarized light », J. Biomed. Opt., vol. 7, no 3, p. 329-340, jul. 2002, doi: 10.1117/1.1484498.

[25] M. Anastasiadou et al., « Polarimetric imaging for the diagnosis of cervical cancer », Phys. Status Solidi C, vol. 5, no 5, p. 1423-1426, 2008, doi: 10.1002/pssc.200777805.

[26] S. Chae et al., « Machine Learning Model for Complete Reconstruction of Diagnostic Polarimetric Images from partial Mueller polarimetry data », 19 sep. 2024, arXiv: arXiv:2409.13073. doi: 10.48550/arXiv.2409.13073.

[27] S. Chae et al., « Machine Learning Approach to 3×4 Mueller Polarimetry for Complete Reconstruction of Diagnostic Polarimetric Images of Biological Tissues », IEEE Trans. Med. Imaging, vol. 44, no 9, p. 3820-3831, sep. 2025, doi: 10.1109/TMI.2025.3567570.

[28] N. S. B. Azahari et N. Z. B. Harun, « Quantum Cryptography Experiment using Optical Devices », Int. J. Adv. Comput. Sci. Appl. IJACSA, vol. 14, no 1, jan. 2023, doi: 10.14569/IJACSA.2023.0140166.

[29] C. Heinrich, J. Rehbinder, A. Nazac, B. Teig, A. Pierangelo, et J. Zallat, « Mueller polarimetric imaging of biological tissues: Classification in a decision-theoretic framework », J. Opt. Soc. Am. A Opt. Image Sci. Vis., vol. 35, no 12, p. 2046-2057, dec. 2018, doi: 10.1364/JOSAA.35.002046.

[30] J. Vizet et al., « First Demonstration of in vivo Mueller Polarimetric Imaging on Human Uterine Cervix », in Conference on Lasers and Electro-Optics (2018), paper AM2J.5, Optica Publishing Group, may 2018, p. AM2J.5. doi: 10.1364/CLEO_AT.2018.AM2J.5.

[31] J. Rehbinder et al., « Depolarization imaging for fast and non-invasive monitoring of cervical microstructure remodeling in vivo during pregnancy », Sci. Rep., vol. 12, no 1, p. 12321, jul. 2022, doi: 10.1038/s41598-022-15852-w.

[32] J. Vizet et al., « In vivo imaging of uterine cervix with a Mueller polarimetric colposcope », Sci. Rep., vol. 7, no 1, p. 2471, jun 2017, doi: 10.1038/s41598-017-02645-9.

[33] Mutiullah, M. Bari, A. Ahmed, M. Sabir, et S. Naveed, « Lung Cancer Detection Using Digital Image Processing Techniques: A Review », 2019. https://www.semanticscholar.org/paper/Lung-Cancer-Detection-Using-Digital-Image-A-Review-Mutiullah-Bari/a260a11aa3de8092796b31f6d028be63b4c2fdf5.doi:10.22581/muet1982.1902.10.

[34] D. Claus et al., « Large-field-of-view optical elastography using digital image correlation for biological soft tissue investigation », J. Med. Imaging, vol. 4, no 1, p. 014505, mar 2017, doi: 10.1117/1.JMI.4.1.014505.

[35] M. Sakli, C. Essid, B. B. Salah, et H. Sakli, « Flexible Framework for Lung and Colon Cancer Automated Analysis Across Multiple Diagnosis Scenarios », Int. J. Adv. Comput. Sci. Appl. IJACSA, vol. 16, no 2, feb. 2025, doi: 10.14569/IJACSA.2025.0160258.

[36] L. G. da Silva, W. R. S. da Silva Monteiro, T. M. de Aguiar Moreira, M. A. E. Rabelo, E. A. C. P. de Assis, et G. T. de Souza, « Fractal dimension analysis as an easy computational approach to improve breast cancer histopathological diagnosis », Appl. Microsc., vol. 51, no 1, p. 6, apr. 2021, doi: 10.1186/s42649-021-00055-w.

[37] M. A. Pala, M. E. Çimen, A. Akgül, M. Z. Yıldız, et A. F. Boz, « Fractal dimension-based viability analysis of cancer cell lines in lens-free holographic microscopy via machine learning », Eur. Phys. J. Spec. Top., vol. 231, no 5, p. 1023-1034, jun 2022, doi: 10.1140/epjs/s11734-021-00342-3.

[38] Z. U. Nisa, A. Jaffar, S. M. Bhatti, et U. M. Butt, « Lung Cancer Detection using Segmented 3D Tensors and Support Vector Machines », Int. J. Adv. Comput. Sci. Appl., vol. 14, no 10, 2023, doi: 10.14569/IJACSA.2023.0141066.

[39] D. Klyushin, K. Golubeva, N. Boroday, et D. Shervarly, « Breast Cancer Diagnosis Using Machine Learning and Fractal Analysis of Malignancy-Associated Changes in Buccal Epithelium », in Artificial Intelligence, Machine Learning, and Data Science Technologies, CRC Press, 2021.

[40] F. E. Lennon et al., « Lung cancer—a fractal viewpoint », Nat. Rev. Clin. Oncol., vol. 12, no 11, p. 664-675, nov. 2015, doi: 10.1038/nrclinonc.2015.108.

[41] L. Wei, Q. Gan, et T. Ji, « Cervical cancer histology image identification method based on texture and lesion area features », Comput. Assist. Surg. Abingdon Engl., vol. 22, no sup1, p. 186-199, dec. 2017, doi: 10.1080/24699322.2017.1389397.

[42] K. V. Ranjitha et T. P. Pushphavathi, « Analysis on Improved Gaussian-Wiener filtering technique and GLCM based Feature Extraction for Breast Cancer Diagnosis », Procedia Comput. Sci., vol. 235, p. 2857-2866, jan. 2024, doi: 10.1016/j.procs.2024.04.270.

[43] M. Mawarni, F. Utaminingrum, et W. F. Mahmudy, « The Effect of Feature Selection on Gray Level Co-Occurrence Matrix (GLCM) for the Four Breast Cancer Classifications », J. Biomim. Biomater. Biomed. Eng., vol. 55, p. 168-179, 2022, doi: 10.4028/p-09g3n8.

[44] R. L. Hasanah et D. Riana, « Classification of Dermoscopic Image of Skin Cancer Using the GLCM Method and Multi-SVM Algorithm », Rekayasa, vol. 14, no 3, p. 407-415, dec. 2021, doi: 10.21107/rekayasa.v14i3.12213.